Consistent look-up table interpolation method for real-gas flow simulations

M. Pini [a,*], A. Spinelli [b], G. Persico [b], S. Rebay [c]

[a] Delft University of Technology, Aerospace Engineering Faculty, Propulsion and Power, Kluyverweg 1, 2629 HS Delft, The Netherlands
[b] Politecnico di Milano, Department of Energy, via Lambruschini 4, 20156 Milano, Italy
[c] Universitá di Brescia, Department of Mechanical and Industrial Engineering, via Branze 38, 25123 Brescia, Italy

Received 28 March 2014
Received in revised form 26 October 2014
Accepted 2 November 2014
Available online 18 November 2014

1. Introduction

The accurate modeling of thermodynamic and transport properties of fluids exhibiting non-negligible real-gas behavior is crucial in many technical applications; in energy-conversion systems fluids are often employed far from ideal gas conditions, and the availability of proper thermodynamic models is a necessary prerequisite for the accurate estimate of both component and whole-system performance. The prediction of real-gas thermodynamic properties can be achieved by determining analytical expressions for the fundamental relation or, more commonly, by resorting to Equations of State (EoS) and their derivatives. Several formulations of the EoS and of transport properties correlations are available [24,20,12,14,4,3,6], but their use through thermodynamic libraries [7] is computational expensive in case of numerical studies, when a set of governing equations is iteratively solved, e.g., detailed Computational Fluid Dynamic (CFD) calculations [10], dynamic plant simulations [18].

As an alternative, Look-up Tables (LuT) can be adopted to represent the thermo-physical behavior of the fluid. The LuT concept is fairly simple; in the thermodynamic region of interest, a grid of nodal points (storing all thermodynamic and transport properties) is preliminary built and the properties at any other point are computed using fast interpolation methods, with a dramatic reduction in computational time [11,13,2,22]. However, standard LuT approaches do not automatically satisfy thermodynamic consistency, as it is guaranteed by the use of analytical EoS. Referring to a pure substance or to a mixture of given composition, thermodynamic consistency implies that, given a triple of thermodynamic

* Corresponding author. Tel.: +31 (0)15 27 84794.
E-mail address: M.Pini@tudelft.nl (M. Pini).

properties, e.g. P, T, ρ, if $T = g(P, \rho)$ and $P = f(T, \rho)$, then $P \equiv f(g(P, \rho), \rho)$. Generally, most of the LuT approaches substitute the functions f, g with their approximate counterparts $\tilde{f}, \tilde{g}$ and this finally leads to $P \not\equiv f(g(P, \rho), \rho)$. The consistency error $\epsilon = P - \tilde{f}(\tilde{g}(P, \rho), \rho)$ can be minimized by increasing the accuracy of the LuT, improving either the number of mesh nodes or the order of the interpolation scheme. This can be usually done at the expense of a greater computational cost. On the other hand, consistency errors may induce significant non-smooth perturbations over CFD code iterations, which may even prevent the solver to converge.

This paper presents a novel interpolation method for property calculation of real gases using LuT. At first, the values of specific internal energy e, expressed in terms of specific entropy s and specific volume v, are calculated for each node of the grid by exploiting the accurate EoS implemented in the software *FluidProp* [7]. Then, the nodal values are utilized to construct, once assigned a certain functional dependency, a fundamental relation in the energy form $e = e(v, s)$, one for each cell of the thermodynamic domain. More specifically, the set of closure coefficients pertaining to a single fundamental relation is determined by interpolation on the closest grid data, according to the order of the function. Lastly, the algorithm provides the thermodynamic properties by conveniently combining the derivatives of the fundamental relation. The method results to be compactly supported, i.e. it has local nature, it can be retained semi-analytical, and primarily guarantees that any thermodynamic property of any internal point is consistently calculated. Nevertheless, to avoid failures during property calculation, the functional form chosen for e needs to exhibit a sufficient regularity (derivatives up to second order are usual for process or fluid-dynamic calculations) and must fulfill the thermodynamic stability within the cell.

A similar approach is adopted for obtaining the transport properties. Two different functional forms are prescribed for the dynamic viscosity μ and for the thermal conductivity k; coherently with the thermodynamic table, also the transport properties are expressed as functions of the specific volume and of the specific entropy $\mu = \mu(v, s)$, $k = k(v, s)$. Correspondingly, the set of coefficients of the two interpolating functions is resolved at any cell on the basis of the transport properties stored inside the grid points. Since such values are computed (starting from two independent thermodynamic properties) by resorting to semi-empirical relations, no consistency issues have to be taken into account, providing that positive values are achieved.

The paper is structured as follows: the theoretical background of the novel LuT methodology is initially outlined in Section 2. Issues concerning thermodynamic stability, accuracy and computational cost are discussed in Section 3, in which the LuT method is applied to the siloxane MDM and the carbon dioxide; both single and two-phase regions close to the vapor saturation line are explored, for reduced temperatures ranging between $T_r \simeq 0.6$ and $T_r \simeq 1.05$. To conclude, two examples of LuT application in combination with CFD simulation are extensively presented in the latest Section 4.

2. Look-up Table approach (LuT)

The standard computational scheme of any interpolation based method for the calculation of thermo-physical properties consists of a two-step procedure. As a first step, the thermodynamic mesh is generated based on the data provided by an existing database (tables of experimental data or even Equations of State and transport properties correlations). The whole set of properties is computed afterwards on the basis of the data stored in each node of the grid. The key aspects of a LuT algorithm, namely its efficiency and its accuracy, are then related to the methodologies introduced to resolve either steps. This section presents the methods devel-oped in this work to achieve an optimal compromise between accuracy and computational cost, given that the thermodynamic consistency is intrinsically satisfied.

Differently from current LuT approaches, the present method allows to compute the thermodynamic quantities on physical basis, i.e. the properties stored in the nodes of the table are used to construct (by proper interpolation) local fundamental relations, which are analytically differentiated to retrieve the properties of interest –P, T, c, ...– in a straightforward manner. Each step of the procedure is separately described in the following.

2.1. Generation of the thermodynamic mesh

The construction of the thermodynamic mesh is based on the discretization of the saturation line according to a given temperature interval. The points can be uniformly or variably spaced through a spline-based reconstruction method, allowing also a refinement as the critical point is approached; an example of discretized vapor saturation line for siloxane *MDM* is given in Fig. 1. The resulting saturation grid represents the support line on which the LuT is constructed by proceeding along directions locally orthogonal to the line.

The normal spacing may be, in principle, specified using a generic pair of states (e.g. ρ, e), however, this choice strongly affects the shape and the thermodynamic regions covered by the resulting grid. Fig. 2 depicts three different thermodynamic meshes generated starting from the same basis points and specifying the normal spacing as a function of $log(v)$, s, $log(T)$, s, and $log(v)$, e. As well visible, the third grid extends in regions far from the critical point, while the former two also include the supercritical zone; this represents a crucial advantage in processes that occur, at least

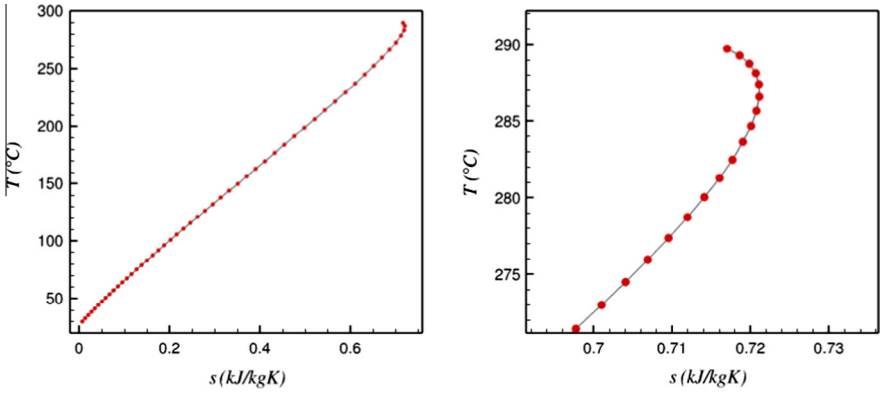

Fig. 1. Left: Discretized MDM vapor saturation line in the T–s plane. Right: Discretized MDM vapor saturation line in the critical region of the T–s plane.

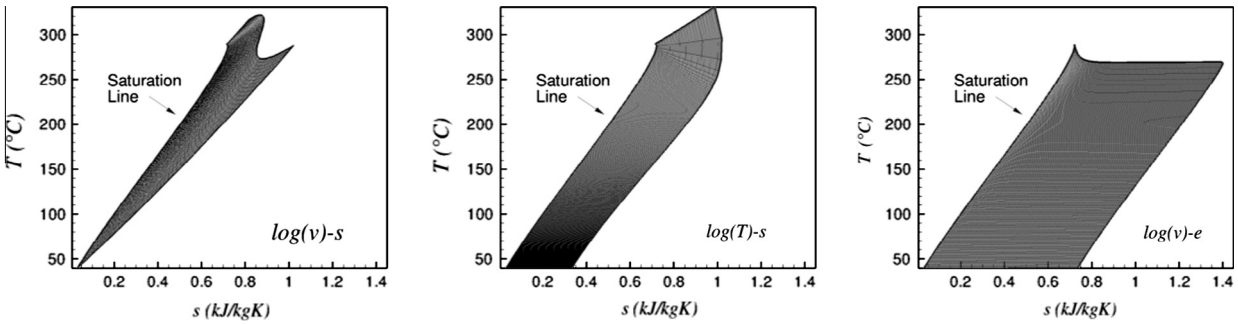

Fig. 2. Thermodynamic meshes generated using $log(v),\ s,\ log(T),\ s$, and $log(v),\ e$ as independent variables for normal spacing. For clarity, the tables are reported in the T–s plane.

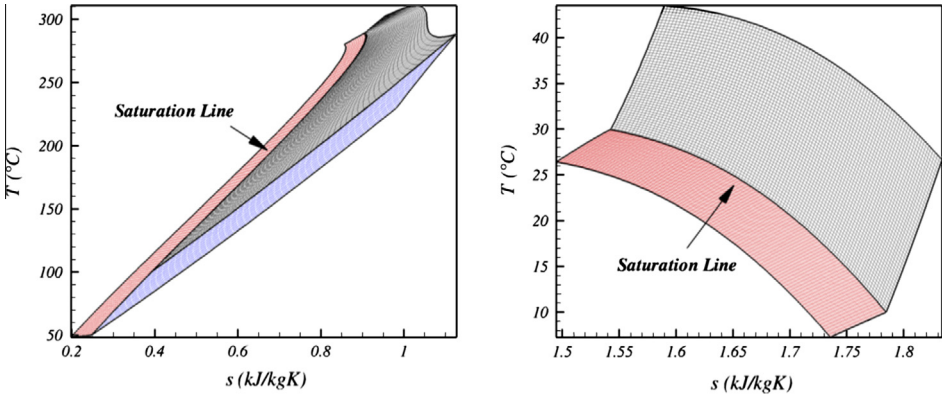

Fig. 3. Look-up Tables for siloxane MDM (left) and CO_2 (right) in the T–s plane.

partially, in the dense-gas region, such as organic Rankine cycles (ORC) turbine expansions. Furthermore, the use of $log(T),\ s$ as independent variables usually leads to relevant deformations of the mesh for different couples of thermodynamic properties. This results in higher computational costs and lower accuracies when the LuT method is applied in process or CFD calculation, in which different couples (e.g. ρ, e or P, ρ) are required. After several trials on a large variety of fluids, the definition of the normal spacing in the $log(v), s$ plane resulted as the best construction strategy. This allows to easily embed real gas regions in the thermodynamic domain, while preserving an acceptable skewness of the mesh for the couples commonly required in CFD calls. As a result, $log(v),\ s$ represents the basic choice of all grids constructed for the CFD simulations reported in the following.

The use of the saturation line as a basic support for LuT construc-tion enables also the adoption of a multi-block approach, providing that the saturation line is split into several pieces, possibly with dif-ferent discretization. The multi-block construction also allows to easily embed two-phase regions in the domain; the adjacent blocks result completely separated, with two different sets of points (one for each block) assigned at the boundary. All properties are contin-uous across any single cell of the domain, since (by construction) none of them can be crossed by the saturation line. Fig. 3 sketches, in the T–s plane, two examples of thermodynamic mesh for, respec-tively, *MDM* (split into three blocks) and CO_2 (made by two blocks). As the original tables are generated in the $log(v), s$ plane, the corre-sponding grids in the T, s plane may exhibit a certain skewness, especially for fluids featuring a positive slope of the saturation line such as *MDM*. Notice also that mesh spacing can differ from one block to another and in both grid directions (e.g., Fig. 3, left).

2.2. Construction of the fundamental relation

The major novelty of the present approach is the construction of a thermodynamic fundamental relation in the form $e = e(v, s)$ valid within each cell through an interpolation-based method. The pre-computed thermodynamic properties (stored at any grid node) are used as basis points. An analytic functional form is then required to mimic the real thermodynamic behavior of the fluid. In this context a simple bilinear and a more accurate bicubic bivariate interpolation methods based on edge-points are implemented. In particular the bicubic form was chosen in such a way to guarantee a degree of variability of the second derivatives within the cells; as a matter of fact the second derivatives of the fundamental relation are required for the calculation of some thermodynamic quantities, such as the specific heats or the speed of sound, as shown in Section 2.4. The bicubic functional form can be written as

$$e(v,s) = \sum_{j=0}^{N}\sum_{i=0}^{M} b_{i,j}\, v^i s^j \quad N = 3,\ M = 3 \tag{1}$$

For each cell the coefficients $b_{i,j}$ of the interpolation functions are determined by using the values of entropy, specific volume, and internal energy of the surrounding 4 (bilinear) or 16 (bicubic) grid nodes.

This approach allows to manage the calculation of the whole set of weights for all grid cells in a pre-processing phase. As a result, the accuracy of the method may be further enhanced by using higher-order interpolating functions without compromising the computational efficiency of the calculation strategy; indeed, the overall expense remains only dependent on the number of cells and on the pair of state variables, as outlined in the following.

2.3. Transport property functional forms

Similarly to the case of thermodynamic properties, the transport properties of any point of the domain are calculated according to a LuT approach. Therefore, a local analytical functional form is constructed for both the dynamic viscosity μ and the thermal conductivity k at any cell of the grid. In either cases the specific volume v and the specific entropy s have been taken as independent variables and simple bilinear functions are implemented, since no second order derivatives of transport properties are required in the context of fluid-dynamic computations. However, more complex relations can be adopted with no significant increase of the computational cost. The bilinear functional forms for μ and k can be written as:

$$\mu(v,s) = \sum_{j=0}^{N}\sum_{i=0}^{M}\beta_{i,j} v^i s^j \quad N=1,\ M=1 \tag{2}$$

$$k(v,s) = \sum_{j=0}^{N}\sum_{i=0}^{M}\zeta_{i,j} v^i s^j \quad N=1,\ M=1 \tag{3}$$

Each set of local coefficients $\beta_{i,j},\ \zeta_{i,j}$ is established by taking the triple $v,\ s,\ \mu$ or $v,\ s,\ k$ of the surrounding 4 grid nodes. As in the case of thermodynamic property calculation, the whole set of weights is determined in the pre-processing phase, thus not affecting the computational efficiency of the method.

2.4. Computation of thermodynamic properties

The whole set of thermodynamic quantities normally involved in process or fluid-dynamic calculations, e.g., $P,\ T,\ h,\ c,\ c_v,\ c_P$, is provided by properly deriving the analytical expression of the fundamental relation. As a result, the thermodynamic consistency of the method is automatically satisfied. Since the speed of sound and the specific heats are functions of the second-order partial derivatives of e, the bicubic interpolation form is suited for the solution of flow problems. The full set of thermodynamic properties as a function of $s,\ v$ can be written as

$$\begin{aligned}
P &= -\left(\frac{\partial e}{\partial v}\right)_s,\\
T &= \left(\frac{\partial e}{\partial s}\right)_v,\\
h &= e - \left(\frac{\partial e}{\partial v}\right)_s v,\\
c &= v\sqrt{\left(\frac{\partial^2 e}{\partial v^2}\right)_s},\\
c_v &= \frac{T}{\left(\frac{\partial^2 e}{\partial s^2}\right)_v},\\
c_P &= \frac{T\left(\frac{\partial^2 e}{\partial v^2}\right)_s}{\frac{T}{c_v}\left(\frac{\partial^2 e}{\partial v^2}\right)_s - \left(\frac{\partial^2 e}{\partial v \partial s}\right)^2},
\end{aligned} \tag{4}$$

in which c_P is only defined in single phase regions. Furthermore, most of the flux splitting numerical schemes suitable for arbitrary equations of state, as the one proposed in [25] and implemented in the flow solvers described in the following, require the calcula-tion of secondary thermodynamic properties to reconstruct the fluxes among adjacent cells. These are commonly limited to deriv-atives of pressure with respect to density and to internal energy for inviscid simulations [5], which, properly combined, are used to recover the fluid speed of sound. The specification of temperature derivatives is further needed in case of viscous [19] and through-flow problems [16] solved by implicit time integration algorithms.

If analytically rewritten as function of $s,\ v$, such derivatives can be additionally obtained as outcome of the present LuT method as follows:

$$\begin{aligned}
\left(\frac{\partial P}{\partial e}\right)_\rho &= -\frac{1}{T\left(\frac{\partial^2 e}{\partial v^2}\right)_s},\\
\left(\frac{\partial P}{\partial \rho}\right)_e &= \frac{c^2}{c^2 + \left(\frac{\partial P}{\partial e}\right)_\rho \left(\frac{\partial e}{\partial v}\right)_s v^2},\\
\left(\frac{\partial T}{\partial e}\right)_\rho &= \frac{\left(\frac{\partial^2 e}{\partial s^2}\right)_v}{T},\\
\left(\frac{\partial T}{\partial \rho}\right)_e &= -\frac{v^2}{\frac{\partial^2 e}{\partial v \partial s}}.
\end{aligned} \tag{5}$$

For a given input pair of thermodynamic properties (e.g. $vs,\ ve,\ Ps,\ PT$) the calculation strategy is divided into three main steps: the mesh cell containing the desired point is initially identified and the corresponding set of coefficients $b_{i,j}$ is separately selected; then the given pair is converted into the explicit state v, s by iteratively solving a non-linear equation (system); finally the thermodynamic properties are calculated by means of the set of Eqs. (4) and (5).

The identification of the correct grid element where the thermodynamic point of interest lies represents the most demanding operation of any LuT approach and the time correspondingly required proportionally increases with the number of mesh nodes. A considerable reduction of the computational expense related to the search process is herein achieved by adopting fast nearest-neighbor techniques. Within the present LuT algorithm a robust *kd-tree* partitioning algorithm [1,21] has been implemented and tuned to decompose the original thermodynamic domain in a tree structure suitable for a highly efficient search procedure.

In particular, several tree structures are assembled and stored, one for each couple of thermodynamic states required in CFD codes. Such an approach leads to approximately the same computational cost for a single search procedure using different input pairs, at least on meshes characterized by similar skewness. Moreover, as *kd-tree* methods act primarily on Euclidean spaces, an algebraic transformation is initially applied to the thermodynamic properties in order to map the original values within the normalized space 0–1. This ensures an acceleration of the searching process.

Apart from the favorable case of $v,\ s$, which seldom occurs in CFD or process calculations, any other pair of states cannot be directly used for the computation of the thermodynamic properties, as the fundamental relation explicitly depends on $v,\ s$. Therefore the input state has to be preliminarily converted into the independent state $v,\ s$ by solving a non-linear problem in the form $\mathbf{f}(v,s) = \mathbf{f}_0,\ \mathbf{f}_0$ being a vector of two given properties. The most demanding case occurs when none of the input variables correspond to the independent variables of the fundamental relation. Considering for example $P,\ T$ as independent variables, the non-linear system to be solved to restore $v,\ s$ can be written as

$$\begin{aligned}
P(v,s) &= P_0,\\
T(v,s) &= T_0.
\end{aligned} \tag{6}$$

Eq. (6) can be solved by any iterative algorithm available for non-linear systems. In this work some Newton's updates are employed to hasten the solution. The linearization of Eq. (6) simply holds

$$\begin{aligned}
P(v+\delta v, s+\delta s) &= P(v,s) + \frac{\partial P}{\partial v}\delta v + \frac{\partial P}{\partial s}\delta s = P_0,\\
T(v+\delta v, s+\delta s) &= T(v,s) + \frac{\partial T}{\partial v}\delta v + \frac{\partial T}{\partial s}\delta s = T_0.
\end{aligned} \tag{7}$$

By plugging the fundamental relation into the linearized equations, the full system is more conveniently expressed as

$$\begin{bmatrix} \frac{\partial P}{\partial v} & \frac{\partial P}{\partial s} \\ \frac{\partial T}{\partial v} & \frac{\partial T}{\partial s} \end{bmatrix} \begin{bmatrix} \delta v \\ \delta s \end{bmatrix} = \begin{bmatrix} \frac{\partial^2 e}{\partial v^2} & -\frac{\partial^2 e}{\partial v \partial s} \\ \frac{\partial^2 e}{\partial v \partial s} & \frac{\partial^2 e}{\partial s^2} \end{bmatrix} \begin{bmatrix} \delta v \\ \delta s \end{bmatrix} = \begin{bmatrix} P_0 - P(v,s) \\ T_0 - T(v,s) \end{bmatrix}, \tag{8}$$

where the vector $\delta v,\ \delta s$ represent the incremental steps of the solution $v,\ s$. A very fast convergence is usually achieved by selecting as initial guess for the iterative process the couple $v,\ s$ belonging to the mesh node closest to the assigned one. Given the couple $v,\ s$ corresponding to the point of interest, the thermodynamic quantities are straightforwardly evaluated by applying the relations (4), while the transport properties are simply given by the functional forms (2) and (3).

3. Analysis of the method

In this section the accuracy and the computational efficiency of the method are carefully assessed, alongside a discussion about the thermodynamic stability of the local fundamental relations. Carbon dioxide and siloxane *MDM* are considered as reference compounds for the investigations. The thermodynamic tables are constructed on the basis of the data based on the reference EoS implemented in *FluidProp*.

3.1. Thermodynamic stability

Each fundamental relation describing thermodynamic equilibrium states has to satisfy the so-called stability conditions [9]. To guarantee the thermodynamic stability it is necessary and sufficient that the fundamental relation is convex with respect to the specific entropy and the specific volume, namely that, for a pure substance:

$$d^2e = \frac{1}{2}\left(\frac{\partial^2 e}{\partial s^2}\right)_v ds^2 + \left(\frac{\partial^2 e}{\partial s \partial v}\right) ds\, dv + \frac{1}{2}\left(\frac{\partial^2 e}{\partial v^2}\right)_s dv^2 > 0 \tag{9}$$

Therefore, the quadratic form (9) which expresses d^2e is required to be positive definite or, equivalently, that all the principal minors of the matrix of the quadratic form are positive. As the matrix of (9) is the Hessian matrix $(H = H(s, v))$ of e, the stability of the fundamental relation is guaranteed if and only if [9]:

$$\begin{cases} H_{1,1} = \left(\frac{\partial^2 e}{\partial s^2}\right)_v > 0 \\ det(H) = \left(\frac{\partial^2 e}{\partial s^2}\right)_v \left(\frac{\partial^2 e}{\partial v^2}\right)_s - \left(\frac{\partial^2 e}{\partial s \partial v}\right)\left(\frac{\partial^2 e}{\partial v \partial s}\right) > 0. \end{cases} \tag{10}$$

The bicubic relation expressed in (1), therefore, must guarantee the thermodynamic stability in the region of application. This simply leads to local conditions, since a different fundamental relation is defined on a single mesh element. As a result, a simple method to ensure the local stability of a given bicubic function requires the verification of the conditions specified by (10) over the domain of application. In the present work this operation is performed immediately after the definition of the full set of bicubic relations. In particular, the stability conditions have been investigated in additional verification points obtained by equally dividing each cell of the support mesh in eight parts. These points include the barycenter of the cells, which represent the points where the interpolation error tends to be higher. The fulfillment of the stability conditions have been satisfactorily verified for different fluids and for mesh of different dimensions over the entire (possibly multi-block) domain. Fig. 4 shows, in the T–s diagram, how the stability conditions are fulfilled by the whole set of fundamental relations established in the domain using the LuT. The results reported in Fig. 4 refer to a two-block LuT constructed for the silox-ane MDM using 5000 cells for the single-phase block and 2500 cells for the two-phase block. The verification points are about 40,000 for the vapor/supercritical region and about 20,000 for the two-phase region. It can bee seen how conditions (10) are respected at any investigated point of the thermodynamic domain and not only on the support grid nodes, as already guaranteed by the stability of the Span–Wagner EoS [4] employed for the gener-ation of the mesh.

3.2. Accuracy

The accuracy of the proposed LuT approach is herein evaluated by quantitatively estimating the deviations of the interpolated values against the quantities given by the native model implemented in the *FluidProp* database, i.e. the Span–Wagner model for both fluids [4,23], referred to as FP-SW in the sequel. Two ensembles of N_p 500 randomly distributed points are initially generated and used for the analysis. The former group is representative of the regions far from the critical point, the latter one is conversely extrapolated from the critical one. The results shown in the following report the Mean Relative Error (MRE) of $\Psi = (P, c, c_P, \ldots)$, defined as

$MRE = 100 \frac{\sum_{i=1}^{N_p} \|(\Psi_{i_{LuT}} - \Psi_{i_{FP-SW}})/\Psi_{i_{LuT}}\|}{N_p}$, as a function of the grid node number for $v,\ s$ as input pair. Further calculations, not reported herein, gave similar outcomes for the remaining couples.

Figs. 5 and 6 display the convergence of the mean relative error as a function of the table nodes. For both fluids, the error tends to be higher in the critical region. This behavior is most probably due

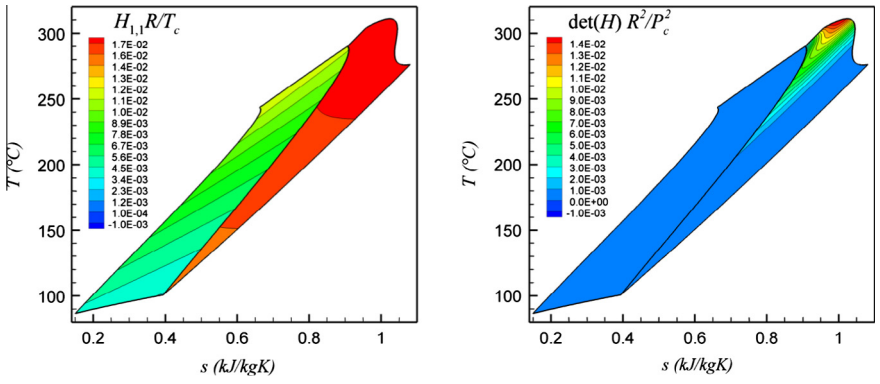

Fig. 4. Verification of the thermodynamic stability for the siloxane MDM. Left: Non-dimensional value of $H_{1,1}$. Right: Non-dimensional value of det(H). $H = H(s, v)$ is the Hessian matrix of the fundamental relation $e = e(s, v)$ established at a certain cell of the domain. Scales are extended to negative values to highlight that only positive quantities are obtained.

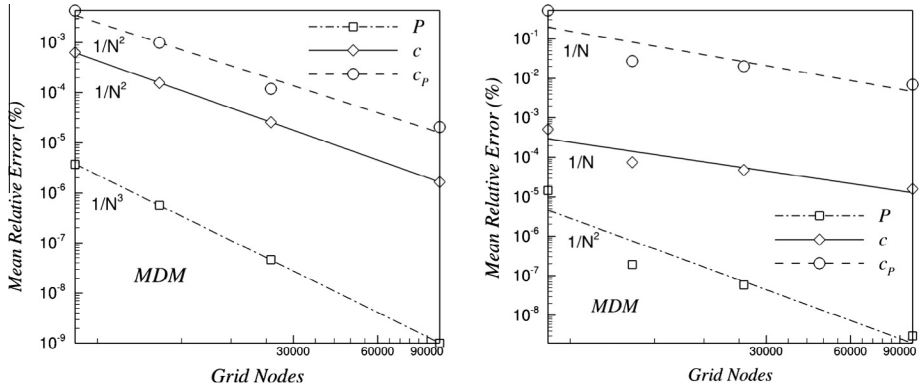

Fig. 5. LUT accuracy for MDM. Left: Mean relative error far from the critical point. Right: Mean relative error in the critical region.

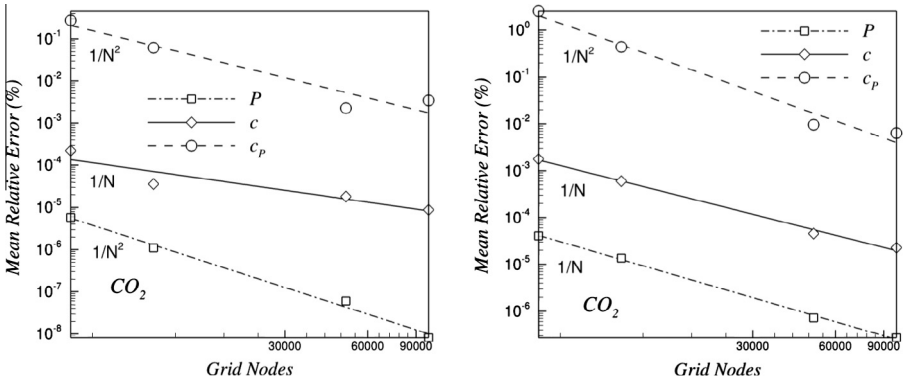

Fig. 6. LUT accuracy for CO_2. Left: Mean relative error far from the critical point. Right: Mean relative error in the critical region.

to strong real gas effects, which induce high deviations of the thermo-physical properties between two close states. As a consequence, the bicubic shape is less suitable to predict the trend of internal energy within a single cell element, resulting in a degradation of the accuracy of its first and second-order derivatives. As expected, Figs. 5 and 6 also show a lower accuracy for c and c_P. This can be easily explained by inferring the order of the interpolating polynomials used for approximating the three properties. Such orders, with respect to the independent variables, can be synthetically written as

$$\begin{aligned} P &\propto v^2, \\ c &\propto v^{\frac{3}{2}}, \\ c_P &\propto s. \end{aligned} \tag{11}$$

As shown, pressure (and temperature) are described by quadratic functions, whereas specific heat capacities are basically linear and, therefore, result to be calculated with minor accuracy. In general the interpolation error decreases quadratically $(1/N^2)$ with the number of mesh elements N far from the critical point, whereas lower convergence orders are achieved in proximity of the critical region.

3.3. Computational efficiency

The computational efficiency of the LuT approach is now assessed by comparing the time necessary for a direct evaluation of the thermo-physical properties using *FluidProp* with that required by the LuT algorithm. The mean ratio of the computational burdens of the two methods (LuT cost divided by the direct evaluation cost) for the set of the previously described 500 points, randomly distributed in the thermodynamic space (in both critical and non-critical regions) is summarized in Tables 1 and 2. For a given input pair the whole set of thermodynamic and transport quantities is evaluated on a fixed thermodynamic mesh composed by 10,000 elements. The computational cost to generate the tables, including the construction of the fundamental relations, has been found relatively cheap, the time being less than a second for both fluids on a single core Intel Xeon 3.6 GHz workstation.

The present interpolation-based scheme outperforms the direct evaluation method for any pair of thermodynamic states. The computational cost reduces up to three orders of magnitude with respect to direct calls where v, s (or one of them) explicitly appears as input state. Up to three orders of magnitude gain can be achieved by calling with v, e in critical regions, which represents the most

Table 1
Mean computational time ratio between the LuT and the FP-SW method far from the critical region.

	vs	*ve*	*Ps*	*PT*
MDM	10^{-3}	10^{-2}	10^{-2}	10^{-1}
CO_2	10^{-3}	10^{-2}	10^{-3}	10^{-1}

Table 2
Mean computational time ratio between the LuT and the FP-SW in the critical region.

	vs	*ve*	*Ps*	*PT*
MDM	10^{-3}	10^{-3}	10^{-2}	10^{-2}
CO_2	10^{-3}	10^{-3}	10^{-3}	10^{-2}

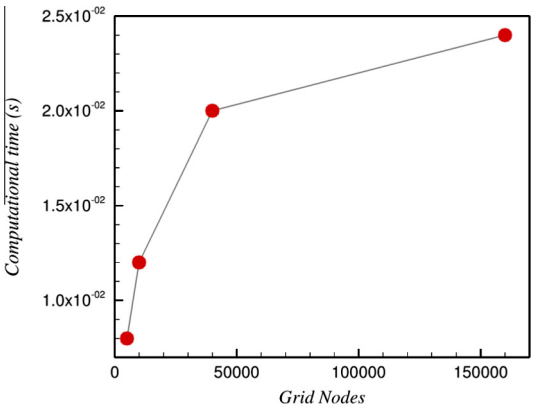

Fig. 7. Total computational cost of 500 search operations carried out for MDM in non-critical regions on grids of varying dimension.

used couple in a CFD solver. Conversely, the use of P, T as independent variables needs the solution of the non-linear system (6), which entails a reduction of the computational gain offered by the LuT method. However, this type of call is not required in real-gas CFD solvers adopting conservative variables.

The influence of the grid dimension on the total computational burden is now investigated. The whole set of thermodynamic properties (previously based on a mesh of 10,000 cells) is assessed against grids of increasing size. The investigation is performed for MDM in the region far from the critical point. The computational expenses are coherently evaluated on meshes having similar skewness.

The results shown in Fig. 7 point out a very interesting trend. The computational cost increases less than linearly with the number of mesh elements, leading to the considerable advantage of making use of very fine mesh, i.e., very accurate properties calculation, without considerably affecting the whole cost of the simulation. Since most of the computational effort is due to the cell identification rather than to the property evaluation (using the same call the evaluation time is almost the same on different grid size), this outcome can be completely conferred to the characteristics of the *kd-tree* partitioning algorithm. In fact, grids covering similar thermodynamic areas but characterized by different number of elements have comparable tree structures, namely the thermodynamic domain is divided in the same number of main partitions. Therefore, the introduction of further mesh points only leads to a modification of the tree structure at a lower level, resulting in an increase of local partitions of the domain for a finer mesh.

Hence, the main architecture of the tree is fully conserved between a coarse and a fine grid, while only its sub-structure is changed. This allows to envisage a search procedure as split in two main parts: the search starts by proceeding along the primary partitions of the tree (global search), which are approximately equal between the two grids, then, in the case of a fine grid, the cell of interest is reached through the peripheral branches (local search) effectively arranged on the main tree structure. For a coarse grid, contrarily, the search stops at the first (global) level; see Fig. 8. The additional time consumed is then only related to the local search, which is usually very efficient. A further investiga-tion conducted by using carbon dioxide provided the same indica-tions. The potential of this feature of the LuT algorithm can be fully exploited in CFD simulations, as those reported in the next section.

4. Application to turbomachinery flows

The proposed LuT method has been embedded into existing CFD solvers for the simulation of turbomachinery flows of organic fluids. In particular TzFlow code [16] for throughflow calculations of multistage machines and zFlow code [5] for blade-to-blade cascade calculations are considered. The performances of both solvers for realistic turbomachinery applications are investigated in the following, considering a transonic multistage radial turbine and a supersonic axial turbine nozzle.

4.1. Throughflow simulation of a multi-stage ORC radial turbine

The throughflow simulation of the transonic six-stage radial turbine proposed in [17], designed to operate with siloxane MDM, is first considered. The calculation presented in [17] was originally performed by coupling the TzFlow solver with the exter-nal thermodynamic library *FluidProp*, which characterizes the MDM fluid with the Span–Wagner model [4]. In the present con-text the TzFlow solver is extended to implement the proposed LuT approach, and then applied to the same machine using tables constructed with the Span–Wagner model, so to guarantee full coherence between the physical models used in the LuT and FP-SW calculations. The comparison between the results achieved with LuT and the FP-SW methods allows to highlight the impact of the thermodynamic treatment on the computational cost and accuracy of a CFD simulation for a whole machine.

The isentropic thermodynamic process ideally experienced by the fluid within the machine is represented in the left frame of Fig. 9, where also the table used for the LuT calculation is provided in the T—s state diagram.

From the fluid dynamic point of view the TzFlow solver implements the so-called CFD-based throughflow model. In a nutshell, the flow model is obtained by averaging the three dimensional Euler equations in the azimuthal direction; this leads to a highly simplified axisymmetric problem, but proper source terms have to be introduced to model the flow deflection imparted by the

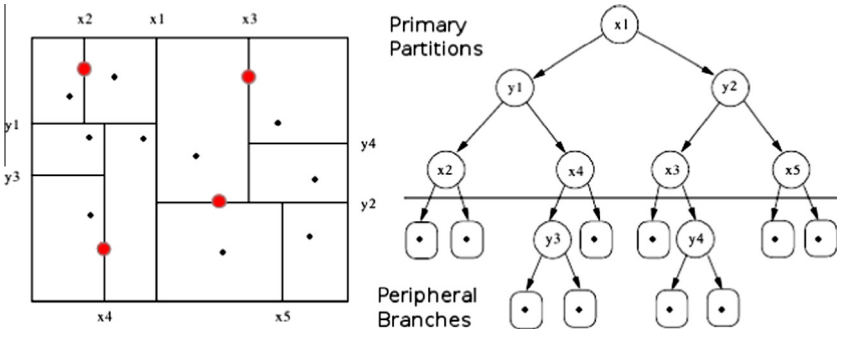

Fig. 8. Overview of kd-tree partitioning algorithm. The values shown are the coordinates of the dividers (red circles), namely the basis points of the table. Black circles indicate the query points. (For interpretation of the references to color in this figure legend, the reader is referred to the web version of this article.)

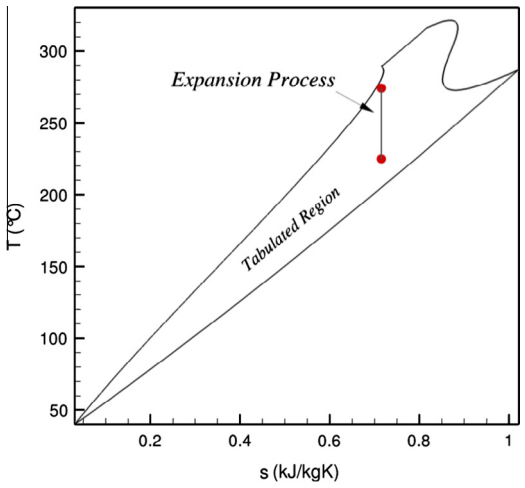

Fig. 9. Tabulated region and expansion line for the throughflow simulation (MDM).

blades, the aerodynamic losses, and the blade blockage [16]. From the thermodynamic point of view the solver is formulated in conservative form, hence the couple e, v represents the input pair in many instances of the calculation; however in the throughflow model the loss source term, formulated as a friction force, is expressed as $D = T \frac{\partial s}{\partial t}$ (with t the streamwise coordinate). As a result, differently from a standard inviscid flow solver, throughflow simulations also require the calculation of temperature, entropy, and their derivatives.

The TzFlow calculations of the six-stage centrifugal turbine have been performed using Craig & Cox loss model [8], and assum-ing elliptic-arc mean line blades (following the design remarks proposed in [15]). The computational grid is composed by about 30 kcells (40×750 cells in spanwise and streamwise direction respectively), arranged in a structured multi-block assembly and composed by cascades and channels; the relatively high number of cells, with respect to the common experience on axisymmetric calculations, is motivated by the spatial resolution required for an appropriate modeling of the gradients of blockage in bladed zones (which holds for the twelve cascades of the machine). For the LuT calculations four thermodynamic tables are considered, composed by 5000, 10,000, 20,000 and 50,000 cells, all of them covering the same area on the state diagram but characterized by different levels of refinement.

An example of result for real-gas throughflow calculations is shown in the left frame of Fig. 10, where the distributions of total enthalpy and entropy on the meridional plane are depicted for the LuT calculation performed with the 5 kcells table. As clearly visible, the total enthalpy only drops across rotors, due to the work exchange (adiabatic flow conditions are assumed, as usually done in turbomachinery); conversely the entropy increases progressively along the machine, due to the action of losses in stator and rotor cascades; both the quantities exhibit large spanwise gradients in the last stages, due to the significant flaring of the channel. All these features are properly captured by both the FP-SW and LuT models, from the quantitative and the qualitative points of view. A relevant quantitative comparison is provided in the right frame of Fig. 10, where the midspan profiles of static pressure and static temperature for FP-SW and LuT models are shown to be perfectly overlapped. This proves that the LuT algorithm (with the specific grid used) is accurate as much as the underlying FP-SW equation in providing the evolution of thermo-physical quantities along the machine.

The crucial quantitative comparison among different models is now performed in terms of computational efficiency. For this comparison the 5 kcells table has been first considered for the LuT model and, beside the FP-SW model, further calculations have been performed using more simple equations of state, namely the polytropic ideal gas (PIG) and the polytropic Van der Waals (PVdW) laws. These latter models are also available in TzFlow by direct implementation of the EoSs within the solver. It should be noted that this procedure represents the most efficient strategy to determine the thermo-physical properties of a working fluid, as just simple analytical operations are required to solve for the full set of thermodynamic relations. Both polytropic models predict the fluid properties by using a constant specific heat ratio, obtained by conveniently averaging the γ values along the ideal expansion line shown in the left frame of Fig. 10.

Table 3 compares the savings in computational cost with respect to FP-SW (implemented through the external library) provided by the LuT, PIG and PVdW models. Since in a CFD calculation a large amount of resources are required by the integration of the flow equations (e.g., for the calculation of fluxes, the solution of linear system, etc.), to properly analyze the effectiveness of the thermody-namic approach the overall computational cost is conveniently split into two contributions: the first one is the cost needed for the fluid-dynamics calculation, which is a fixed and irremovable fraction of the total expense; the second one is the cost needed for the calculation of thermodynamic properties.

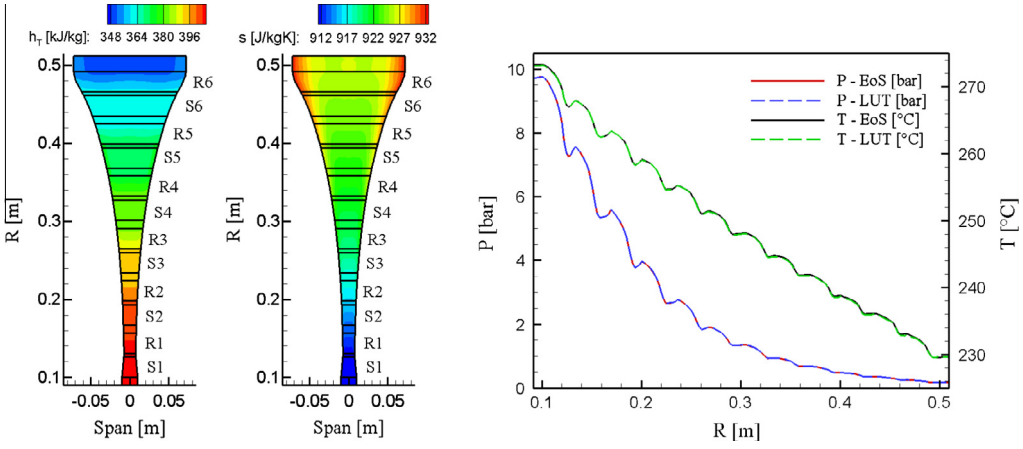

Fig. 10. Left: Meridional evolution of total enthalpy and entropy field within the 6-stage centrifugal turbine. Right: Comparison between FP-SW and LuT results in terms of streamwise distribution of pressure and temperature at turbine mid-span.

Table 3
Total computational cost saved by using different thermodynamic modeling approaches compared to FP-SW model for the throughflow simulation.

	PIG	PVdW	LUT (5 kc)	FP-SW
Time saving	53%	52%	33%	–

Table 4
Total computational cost saved by using different thermodynamic modeling approaches compared to FP-SW model for the supersonic cascade simulation.

	PIG	PVdW	LuT	FP-SW
Time saving	83%	82%	65%	–

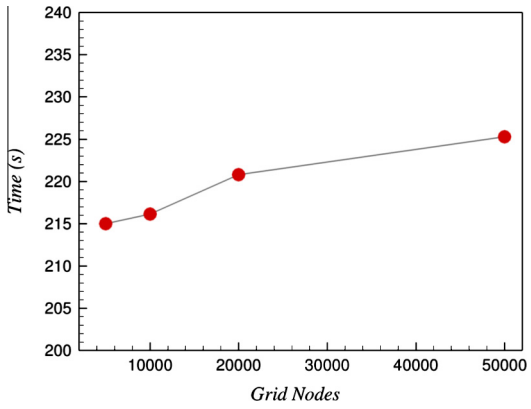

Fig. 11. Total computational cost of the throughflow simulation using different grid size.

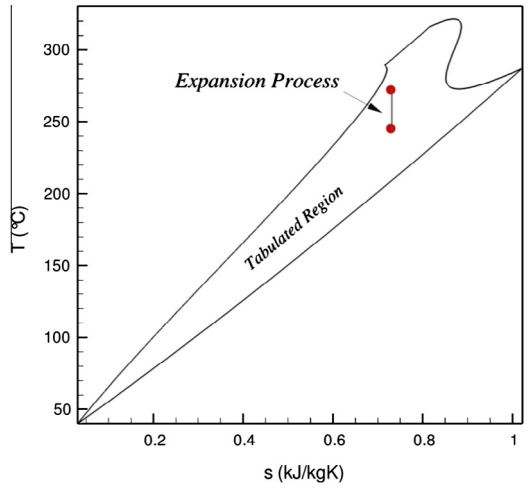

Fig. 12. Tabulated region and expansion line for the axial supersonic turbine simulation (MDM).

For calculations performed using PIG or PVdW models the thermodynamic cost is a few percent of the total one, so their cost represents a rough estimate of the fluid-dynamic cost – the PIG and PVdW simulations share the same computational time indeed, as seen from Table 3. The FP-SW computational cost being the double of the PIG/PVdW one, the thermodynamic cost of the calls to the external library roughly equates the fluid dynamic one. When the LuT approach is used, the fast-searching algorithm and the local analytical model enable to strongly reduce the thermodynamic cost, saving about 2/3 of the corresponding one required by the FP-SW simulation.

The influence of the grid size on the total computational cost of the LuT simulation is now investigated, with reference to the PIG/PVdW computational cost. The three refined grids are used for the comparison, beside the original one. From the data reported in Table 3 it is possible to obtain a rough estimation of a PIG computation, which results approximately 150 s. The difference between the PIG and LuT burdens is around 65 s for a grid of 5 kcells. Increasing the number of grid nodes of one order of magnitude (50 kcells) the extra cost, purely thermodynamic, is just about 13%. As a result the grid size has a slight relevance on the total computational cost of the simulation, allowing for the use of fine (and accurate) thermodynamic meshes, if required by the problem, without compromising the effectiveness of the computational procedure (see Fig. 11).

4.2. Blade-to-blade simulation of a supersonic ORC cascade

The second test case focuses on the blade-to-blade simulation of an axial supersonic ORC nozzle at mid-span. The cascade is characterized by an extremely high expansion ratio, which leads to a design exit Mach number of 2. As a result thereof, the inter-blade channel is of a converging–diverging shape, with a sonic throat upstream of the discharge section. The working compound is siloxane MDM also in this application; the ideal thermodynamic process through the cascade is sketched in Fig. 12, along with the thermodynamic table used for the LuT simulations.

The calculations have been performed with a simplified version of the zFlow code, which solves for the two-dimensional inviscid

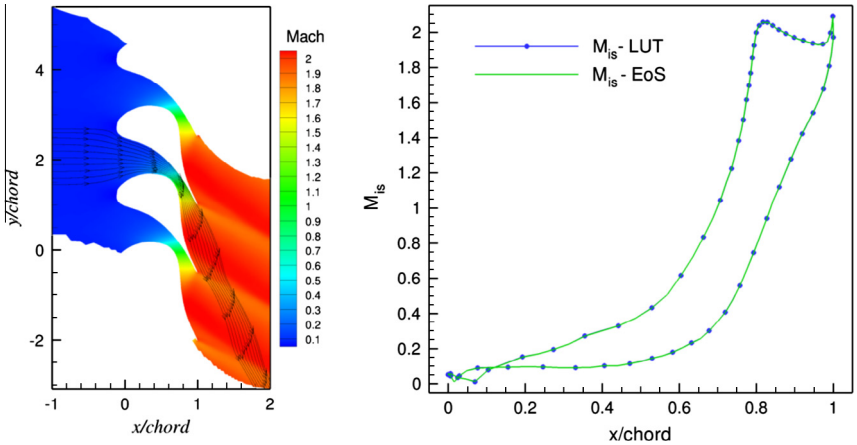

Fig. 13. Left: Blado-to-blade Mach flow field at nominal operating conditions. Right: Predicted isentropic Mach number distribution along the blade surface.

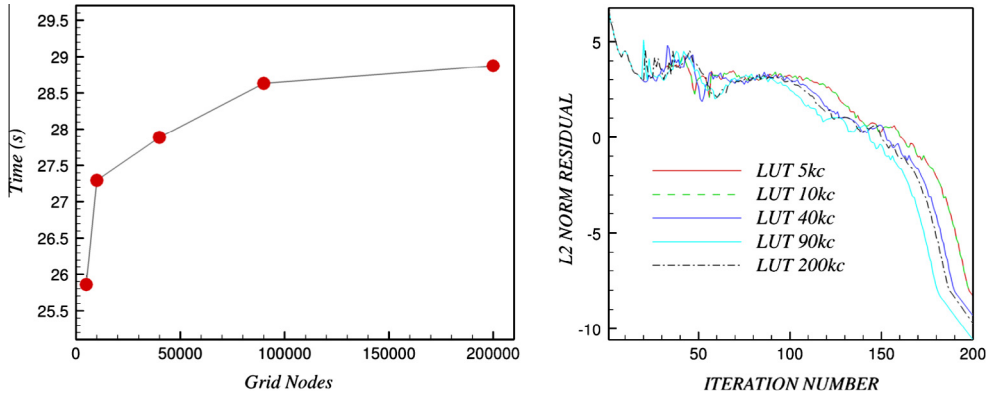

Fig. 14. Left: Total computational cost of the blade-to-blade simulation using different grid sizes. Right: Convergence rate of the flow solver as a function of grid size.

flow equations in Cartesian coordinates; the codes zFlow and TzFlow were developed on the same bases, sharing the same numerical solution procedure and most of the computational features. After a preliminary grid dependence analysis, a computational grid of about 20,000 triangular elements has been selected for the present blade-to-blade calculations; the relatively large number of cells, with respect to typical values used for inviscid blade-to-blade simulations, is motivated by the presence of strong shocks. As done for the previous test case, the results of the LuT approach are now compared with the ones achieved with FP-SW, PIG and PVdW models, first considering a 5 kcells table for the LuT calculation.

The accuracy of the LuT approach is first evaluated against the solution gained by using FP-SW model. The left frame of Fig. 13 shows the distribution of Mach number, from which the sonic throat and the trailing edge shock can be observed. In the same Figure the streamlines are also reported, showing the considerable flow turning both within and, especially, downstream of the blade channel.

Once again, all the flow features are captured by the LuT approach from both the qualitative and quantitative points of view. In particular a relevant quantitative comparison is provided in the right frame of Fig. 13, where the distributions of isentropic Mach number along the blade surface for FP-SW and LuT models are shown to perfectly overlap, confirming the accuracy of the solution provided by the LuT algorithm.

The computational cost and the accuracy of the LuT method are now analyzed. In full coherence with the preceding throughflow application, the same thermodynamic models are herein utilized for the analysis.

The time savings provided by LuT, PIG and PVdW approaches compared to the FP-SW one, reported in Table 4, are larger than that in the throughflow case. In particular, for the FP-SW calculation the thermodynamic cost amounts to 80% of the overall computational cost, considerably higher than that occurring in the throughflow simulation; as a result, the LuT approach provides an even more significant saving, almost the double of that achieved for the throughflow test-case.

As already found for the throughflow calculation, the influence of the table size on the overall computational burden is limited, as depicted in the left frame of Fig. 14; a further study is finally carried out to evaluate the sensitivity of the conver-gence rate on the table size. Very similar residual values are achieved at end of the simulation going from 5 to 200 kcells, as visible in the right frame of Fig. 14. However, lower convergence rates of the flow solver are observed for coarser thermodynamic meshes, as highlighted in the same figure for LuT tables composed by 5 and 10 kcells.

5. Conclusions

This research study has presented an original LuT interpolation method for efficiently managing the calculation of thermo-physical properties. The method has been developed in a fully general manner in order to cope with a variety of pure fluids, mixtures and thermodynamic conditions, i.e., supercritical state, dense-gas, and two-phase flows. Distinguishing features of the proposed approach are the intrinsic thermodynamic consistency and the inherent thermodynamic stability. The performance of the algorithm have been proven through an exhaustive numerical campaign performed at two different levels. First, accuracy and computational efficiency have been carefully evaluated against the results provided by the direct use of EoS, available through the software *FluidProp*, on 500 points randomly distributed in both critical and non-critical region. Second, the method has been coupled with two existing CFD solvers equipped with built-in thermodynamic models (PIG and PVdW) to assess the computational penalty with respect to the use of more simple and less costly EoS.

Both levels of investigation have pointed out the strengths of the method, which revealed high accuracy, high efficiency, and low sensitivity, in terms of computational cost, with respect to grid size. Notably, the last achievement is mainly due to the characteristics of the *kd − tree* search algorithm, which leads the cost of the LuT method to be logarithmically increasing with the number of mesh points. This outcome fosters the adoption of very fine (and accurate) thermodynamic grids for CFD simulations.

References

[1] Boger A. Efficient method for calculating wall proximity. AIAA J 2001;39(12):2404–6. <http://dx.medra.org/10.2514/1.29718>.

[2] Boncinelli P, Rubechini F, Arnone A, Cecconi M, Cortese C. Real gas effects in turbomachinery flows: a computational fluid-dynamics model for fast computations. ASME J Turbomach 2004;126:268–76. <http://dx.medra.org/10.2514/1.29718>.

[3] Chung T-H, Ajlan M, Lee LL, Starling KE. Generalized multiparameter correlation for non-polar and polar fluid transport properties. Ind Eng Chem Res 1988;27:671–9.

[4] Colonna P, Nannan N, Guardone A. Multiparameter equations of state for siloxanes: $[(CH_3)_3–Si–O_{1/2}]_2–[O–Si–(CH_3)_2]_{i=1,3}$, and $[O–Si–(CH_3)_2]_6$. Fluid Ph Eq 2008;263:115–30.

[5] Colonna P, Rebay S. Numerical simulation of dense gas flows on unstructured grids with an implicit high resolution upwind Euler solver. Int J Numer Meth Fluids 2004;46:735–65.

[6] Colonna P, Silva P. Dense-gas thermodynamic properties of single and multicomponent fluids for fluid dynamics simulations. ASME J Fluids Eng 2003;125:414–27. <http://dx.medra.org/10.2514/1.29718>.

[7] Colonna P, van der Stelt TP. FluidProp: a program for the estimation of thermo physical properties of fluids. Software; 2004. <http://www.fluidprop.com>.

[8] Craig HRM, Cox HJA. Performance estimation of axial flow turbines. Proc Inst Mech Eng 1971;185:407–24.

[9] Gyftopoulos EP, Beretta GP. Thermodynamics: foundations and applications. New York: MacMillan Publishing Company; 1991.
[10] Harinck J, Colonna P, Guardone A, Rebay S. Influence of thermodynamic models in 2D flow simulations of turboexpanders. ASME J Turbomach 2010;132:011001–0110017.
[11] Laughman C, Zhao Y, Nikovski D. Fast refrigerant property calculations using interpolation-based methods. In: International refrigeration and air conditioning conference, 2012. p. 10. <http://dx.medra.org/10.2514/1.29718>.
[12] Martin JJ, Hou YC. Development of an equation of state for gases. A I Che J 1955;1(2):142–51.
[13] Pecnik R, Rinaldi E, Colonna P. Computational fluid dynamics of a radial compressor operating with supercritical CO2. ASME J Eng Gas Turb Pow 2012;134:8. <http://dx.medra.org/10.2514/1.29718>.
[14] Peng DY, Robinson DB. A new two-constant equation of state. Ind Eng Chem Fundam 1976;15(1):59–64.
[15] Persico G, Pini M, Dossena V, Gaetani P. Aerodynamic design and analysis of centrifugal turbine cascades. In: ASME turbo expo 2013; 2013. No. GT2013-95770.
[16] Persico G, Rebay S. A penalty formulation for the throughflow modeling of turbomachinery. Comput Fluids 2012;60:86–98.
[17] Pini M, Persico G, Casati E, Dossena V. Preliminary design of a centrifugal turbine for ORC applications. ASME J Eng Gas Turb Pow 2013;135(042312).
[18] Pini M, Spinelli A, Dossena V, Gaetani P, Casella F. Dynamic simulation of a test rig for organic vapours. In: ASME 5th international conference on energy sustainability, ES 2011 (PARTS A, B, AND C); 2011. p. 1977–88.
[19] Rebay S, Colonna P, Pasquale D, Ghidoni A. Simulation of the turbulent dense gas flow through the nozzle of an organic Rankine cycle turbine. In: Heitmeir F, Martelli F, Manna M, editors. 8-th European conference on turbomachinery, fluid dynamics and thermodynamics 23–27 March 2009, Graz-Austria. vol. unico.; March 23–27 2009. p. 1137–48.
[20] Redlich O, Kwong JNS. On the thermodynamics of solutions. V. An equation of state. Fugacities of gaseous solutions. Chem Rev 1949;44(1):233–44.
[21] Roget B, Sitaraman J. Wall distance search algorithm using voxelized marching spheres. J Comput Phys 2013;241:76–94. <http://dx.medra.org/10.2514/1.29718>.
[22] Saaresti-Turunen T, Tang J, Larjola J. A practical real-gas model in CFD. In: European conference on computational fluid-dynamics (ECCOMAS), 2006. p. 9. <http://dx.medra.org/10.2514/1.29718>.
[23] Span R, Wagner W. A new equation of state for carbon dioxide covering the fluid region from the triple-point temperature to 1100 K at pressures up to 800 MPa. J Phys Chem Ref Data 1996;6(24):1509–96.
[24] van der Waals J. Reprinted, on the continuity of gaseous and liquid states, vol. XIV. Amsterdam: North-Holland; 1988.
[25] Vinokur M, Montagnè J. Generalized flux-vector splitting and Roe average for an equilibrium real gas. J Comput Phys 1990;89(2):276–300.